J. Fluid Mech. (2014), *vol.* 754, *pp.* 75–97.
doi:10.1017/jfm.2014.381

Buoyancy scale effects in large-eddy simulations of stratified turbulence

Sina Khani† and Michael L. Waite

Department of Applied Mathematics, University of Waterloo, Waterloo, Ontario, Canada N2L 3G1

(Received 6 March 2014; revised 27 May 2014; accepted 26 June 2014;
first published online 30 July 2014)

In this paper large-eddy simulations (LES) of forced stratified turbulence using two common subgrid scale (SGS) models, the Kraichnan and Smagorinsky models, are studied. As found in previous studies using regular and hyper-viscosity, vorticity contours show elongated horizontal motions, which are layered in the vertical direction, along with intermittent Kelvin–Helmholtz (KH) instabilities. Increased stratification causes the layer thickness to collapse towards the dissipation scale, ultimately suppressing these instabilities. The vertical energy spectra are relatively flat out to a local maximum, which varies with the buoyancy frequency N. The horizontal energy spectra depend on the grid spacing Δ; if the resolution is fine enough, the horizontal spectrum shows an approximately $-5/3$ slope along with a bump at the buoyancy wavenumber $k_b = N/u_{rms}$, where u_{rms} is the root-mean-square (r.m.s.) velocity. Our results show that there is a critical value of the grid spacing Δ, below which dynamics of stratified turbulence are well-captured in LES. This critical Δ depends on the buoyancy scale L_b and varies with different SGS models: the Kraichnan model requires $\Delta < 0.47L_b$, while the Smagorinsky model requires $\Delta < 0.17L_b$. In other words, the Smagorinsky model is significantly more costly than the Kraichnan approach, as it requires three times the resolution to adequately capture stratified turbulence.

Key words: stratified turbulence, turbulence modelling, turbulence simulation

1. Introduction

Stratified turbulence is characterized by very large Reynolds number $Re = u_{rms}l_h/\nu$ and sufficiently small horizontal Froude number $Fr_h = u_{rms}/Nl_h$, such that the buoyancy Reynolds number

$$Re_b = ReFr_h^2, \tag{1.1}$$

is also high (Brethouwer *et al.* 2007). Here, u_{rms} and l_h are the root-mean-square (r.m.s.) velocity and horizontal length scale, respectively; ν is the molecular viscosity and N is the buoyancy frequency. According to Taylor's hypothesis, $l_h \sim (u_{rms})^3/\epsilon$, and so (1.1) yields

$$Re_b \sim \frac{\epsilon}{\nu N^2}, \tag{1.2}$$

† Email address for correspondence: sinakhani@uwaterloo.ca

where ϵ is the kinetic energy dissipation rate (the use of Taylor's hypothesis for stratified turbulence is common, but may be questionable; see e.g. Hebert & de Bruyn Kops 2006*b*; Khani & Waite 2013). The Ozmidov scale (e.g. Lumley 1964)

$$L_o = 2\pi \left(\frac{\epsilon}{N^3}\right)^{1/2}, \tag{1.3}$$

is the smallest scale for which buoyancy effects are important. (We include the 2π factor in (1.3) and for other characteristic length scales because it is often the corresponding wavenumber $k_o = 2\pi/L_o$ that appears in applications; e.g. Gargett, Osborn & Nasmyth 1984; Waite 2011.) Based on the stratified turbulence hypothesis (Lindborg 2006), the Ozmidov scale divides the inertial subrange into two parts: an anisotropic part, from large scales down to the Ozmidov scale; and an isotropic part, for smaller scales down to the Kolmogorov scale $\eta = 2\pi(\nu^3/\epsilon)^{1/4}$. The dynamical picture of stratified turbulence is described by flat horizontal motions and suppressed the vertical velocity, in which the vertical structure is characterized by layers of thickness

$$L_b = 2\pi \frac{u_{rms}}{N}, \tag{1.4}$$

which is named the buoyancy scale (e.g. Riley & de Bruyn Kops 2003; Waite & Bartello 2004; Lindborg 2006). Previous work (e.g. Waite & Bartello 2004; Lindborg 2006; Brethouwer *et al.* 2007; Waite 2011, 2014) shows that the resolution of L_b is necessary to capture the stratified turbulence cascade.

Direct numerical simulation (DNS) of stratified turbulence is very challenging because the ratio of the Ozmidov to Kolmogorov scales depends on the buoyancy Reynolds number as follows

$$\frac{L_o}{\eta} = \left(\frac{\epsilon}{\nu N^2}\right)^{3/4} \sim Re_b^{(3/4)}. \tag{1.5}$$

Since stratified turbulence has $Re_b \gg 1$, and DNS requires resolution of the Kolmogorov scale, it is necessary that the grid spacing be much smaller than the Ozmidov scale. An alternative approach is large-eddy simulation (LES), for which large scales are resolved but subgrid scale (SGS) motions, including the small-scale end of the inertial subrange, are modelled. Owing to the computational costs, we are interested in performing LES of stratified turbulence, in which the grid spacing Δ may be larger than the Ozmidov scale L_o. However, previous numerical studies with hyperviscosity suggest that resolution of the buoyancy scale may be important (e.g. Waite & Bartello 2004; Lindborg 2006; Waite 2011). In this paper, we investigate the performance of two common LES schemes, the Smagorinsky (1963) and Kraichnan (1976) models, in simulations of stratified turbulence. For both schemes, we determine the extent to which the buoyancy scale needs to be resolved for the LES to capture the dynamics of stratified turbulence properly.

In § 2, we review the literature of stratified turbulence, the LES approach, and the classical SGS models. The methodology including numerical approach is outlined in § 3. Section 4 includes results and their interpretations. Concluding remarks are given in § 5.

2. Background

2.1. *Stratified turbulence*

Most previous numerical studies in stratified turbulence are DNS and hyperviscosity simulations. Hyperviscosity simulations are performed in the same spirit as DNS:

the viscosity and diffusion operators are modified to extend the inertial range, but the associated dissipation scale is resolved (e.g. Waite & Bartello 2004). Recent advances in the study of stratified turbulence show that a layerwise structure emerges, in which the horizontal length scale is much larger than the vertical one (e.g. Billant & Chomaz 2001; Riley & de Bruyn Kops 2003; Hebert & de Bruyn Kops 2006*b*; Brethouwer *et al.* 2007). In addition, there is a forward energy transfer mechanism from large to small horizontal scales (e.g. Waite & Bartello 2004; Lindborg 2006; Brethouwer *et al.* 2007). For scales larger than L_o, different kinetic energy spectral slopes have been proposed in the horizontal and vertical directions. Lindborg (2006) argued that $-5/3$ in k_h and -3 in k_v are expected, where $k_h = \sqrt{k_x^2 + k_y^2}$ is the horizontal wavenumber, $k_v = |k_z|$ is the vertical wavenumber, and $\boldsymbol{k} = (k_x, k_y, k_z)$ is the three-dimensional wavevector. When L_b is not resolved in the vertical direction, a steeper horizontal spectrum, with a slope as large as -5, results (e.g. Waite & Bartello 2004). Even when L_b is resolved, deviations from the $-5/3$ slope have been reported; e.g. Waite (2011) and Kimura & Herring (2012) found slopes closer to -2. Moreover, *a priori* testing shows that the horizontal and vertical effective eddy viscosities are very different when the test cutoff wavenumber k_c is smaller than k_o (Khani & Waite 2013). Finally, a non-local horizontal energy transfer from large horizontal scale to the buoyancy scale, associated with Kelvin–Helmholtz (KH) instabilities, has been found in forced stratified turbulence (Waite 2011, 2014), the breakdown of columnar vortices (Augier, Chomaz & Billant 2012), and decaying stratified turbulence (Khani & Waite 2013). All of the results described above have been found when DNS or hyperviscosity simulation is the adopted numerical approach. Despite the emphasis on hyperviscosity and DNS, some LES studies have been investigated (e.g. Siegel & Domaradzki 1994; Carnevale, Briscolini & Orlandi 2001; Smith & Waleffe 2002; Remmler & Hickel 2012; Paoli *et al.* 2013). We are interested in studying LES of stratified turbulence and determining the dependence of the results on the grid spacing Δ.

2.2. *Large-eddy simulations*

LES is based on the filtered equations of motion, where the filter applied to a variable q is given by (e.g. Leonard 1974; Pope 2000)

$$\bar{q}(\boldsymbol{x}, t) = \int_D G(\boldsymbol{x} - \acute{\boldsymbol{x}}, \boldsymbol{x}) q(\acute{\boldsymbol{x}}, t) \mathrm{d}\acute{\boldsymbol{x}}, \tag{2.1}$$

where $\bar{q}(\boldsymbol{x}, t)$ is the filtered quantity, G is a filtering function, which generally depends on $\boldsymbol{x}$ and the distance between two correlation points, i.e. $\boldsymbol{r} = \boldsymbol{x} - \acute{\boldsymbol{x}}$, and D is the spatial domain. In practice, it is customary to work with homogeneous and isotropic filter functions that are independent of $\boldsymbol{x}$ and $\boldsymbol{r}$, and just depend on $r = |\boldsymbol{r}|$. There are a few applicable homogeneous filter functions (see e.g. Pope 2000). For the spectral transform numerical method, it is convenient to work with the sharp spectral filter (as applied in e.g. Germano *et al.* 1991; Moin *et al.* 1991; Piomelli *et al.* 1991; Kang, Chester & Meneveau 2003), which is defined as follows

$$\hat{G}(\boldsymbol{k}) = \begin{cases} 1 : |\boldsymbol{k}| \leqslant k_c \\ 0 : |\boldsymbol{k}| > k_c, \end{cases} \tag{2.2}$$

where $\hat{G}$ is the Fourier coefficient of G, $\boldsymbol{k}$ is the wavenumber vector, and k_c is the cutoff wavenumber. By applying the filter function $\hat{G}$ to variable q, we get

$$\bar{q}(\boldsymbol{x}, t) = \sum_{\boldsymbol{k}} \hat{q}(\boldsymbol{k}, t)\hat{G}(\boldsymbol{k})\mathrm{e}^{\mathrm{i}\boldsymbol{k}\cdot\boldsymbol{x}} = \sum_{|\boldsymbol{k}|\leqslant k_c} \hat{q}(\boldsymbol{k}, t)\mathrm{e}^{\mathrm{i}\boldsymbol{k}\cdot\boldsymbol{x}}, \tag{2.3}$$

where Fourier modes with wavenumbers smaller than k_c are maintained and the larger modes are killed. The LES grid spacing Δ and filter cutoff k_c are related by

$$\Delta \equiv \frac{\pi}{k_c}. \tag{2.4}$$

2.2.1. *Physical space*

Applying the sharp spectral filter to the Navier–Stokes equations under the Boussinesq approximation, which is non-dimensionalized with a velocity scale u and length scale ℓ, yields (following the notation of Pope 2000)

$$\frac{\partial \bar{u}_i}{\partial t} + \frac{\partial}{\partial x_j}(\bar{u}_i\bar{u}_j) = -\frac{\partial \bar{p}}{\partial x_i} - \frac{1}{{Fr_\ell}^2}\bar{\rho}\boldsymbol{e}_z - \frac{\partial \tau^r_{ij}}{\partial x_j} + \bar{f}_i, \tag{2.5}$$

$$\frac{\partial \bar{u}_j}{\partial x_j} = 0, \tag{2.6}$$

$$\frac{\partial \bar{\rho}}{\partial t} + \frac{\partial}{\partial x_j}(\bar{\rho}\bar{u}_j) - \bar{w} = -\frac{\partial h_j}{\partial x_j}, \tag{2.7}$$

where $\boldsymbol{u}$, p, ρ and $\boldsymbol{f}$ are the velocity, perturbation pressure, perturbation density and forcing fields, respectively; and $Fr_\ell = u/N\ell$ is the Froude number. Since we assume large Reynolds numbers and that Δ is much larger than the Kolmogorov scale, viscous dissipation and diffusion are neglected. The subgrid momentum flux $\boldsymbol{\tau}$ and the subgrid density flux $\boldsymbol{h}$ are given as follows

$$\tau_{ij} = \overline{u_iu_j} - \bar{u}_i\bar{u}_j, \tag{2.8}$$

$$h_j = \overline{u_j\rho} - \bar{u}_j\bar{\rho}. \tag{2.9}$$

The deviatoric part of $\boldsymbol{\tau}$ is defined as

$$\tau^r_{ij} = \tau_{ij} - \tfrac{1}{3}\tau_{rr}\delta_{ij}, \tag{2.10}$$

where the modified pressure $\bar{p}$ absorbs the isotropic part of the subgrid momentum flux. The filtered momentum and energy (2.5) and (2.7) are not closed because $\boldsymbol{\tau}^r$ and $\boldsymbol{h}$ are not known in terms of the filtered velocity and density fields. We need to model these unknown fluxes using the SGS models.

2.2.2. *Wavenumber space*

Similar to physical space, we could work in Fourier space to perform LES of stratified turbulence. Applying the sharp spectral filter $\hat{G}(\boldsymbol{k})$ to the Navier–Stokes equations under the Boussinesq approximation in Fourier space yields

$$\frac{\partial}{\partial t}\hat{\bar{u}}_j(\boldsymbol{k}, t) + \frac{1}{{Fr_\ell}^2}\hat{\bar{\rho}}(\boldsymbol{k}, t)\boldsymbol{e}_z = -\mathrm{i}k_m\boldsymbol{P}_{jr}(\boldsymbol{k}) \sum_{\substack{\boldsymbol{p}+\boldsymbol{q}=\boldsymbol{k},\\ |\boldsymbol{k}|<k_c}} \hat{u}_r(\boldsymbol{p}, t)\hat{u}_m(\boldsymbol{q}, t) + \hat{\bar{f}}_j, \tag{2.11}$$

$$k_j \hat{\tilde{u}}_j(\boldsymbol{k}, t) = 0, \tag{2.12}$$

$$\frac{\partial}{\partial t}\hat{\tilde{\rho}}(\boldsymbol{k}, t) - \hat{\tilde{w}}(\boldsymbol{k}, t) = -\mathrm{i}k_m \sum_{\substack{\boldsymbol{p}+\boldsymbol{q}=\boldsymbol{k}, \\ |\boldsymbol{k}|<k_c}} \hat{u}_m(\boldsymbol{p}, t)\hat{\rho}(\boldsymbol{q}, t), \tag{2.13}$$

where $\boldsymbol{P}_{ij} = \delta_{ij} - k_i k_j / k^2$ is the projection tensor, and $k^2 = \boldsymbol{k} \cdot \boldsymbol{k}$. Like in physical space, nonlinear terms in the right-hand side of (2.11) and (2.13), i.e.

$$F_j(\boldsymbol{k}, t) = -\mathrm{i}k_m \boldsymbol{P}_{jr}(\boldsymbol{k}) \sum_{\substack{\boldsymbol{p}+\boldsymbol{q}=\boldsymbol{k}, \\ |\boldsymbol{k}|<k_c}} \hat{u}_r(\boldsymbol{p}, t)\hat{u}_m(\boldsymbol{q}, t), \tag{2.14}$$

$$J(\boldsymbol{k}, t) = -\mathrm{i}k_m \sum_{\substack{\boldsymbol{p}+\boldsymbol{q}=\boldsymbol{k}, \\ |\boldsymbol{k}|<k_c}} \hat{u}_m(\boldsymbol{p}, t)\hat{\rho}(\boldsymbol{q}, t), \tag{2.15}$$

are not known in terms of the filtered Fourier coefficients $\hat{\tilde{\boldsymbol{u}}}$ and $\hat{\tilde{\rho}}$. Based on the definition of the cutoff wavenumber k_c, we could divide (2.14) into a filtered term $\bar{\boldsymbol{F}}$ and a subgrid term $\boldsymbol{F}^s$, such that

$$\bar{F}_j(\boldsymbol{k}, t) = -\mathrm{i}k_m \boldsymbol{P}_{jr}(\boldsymbol{k}) \sum_{\substack{\boldsymbol{p}+\boldsymbol{q}=\boldsymbol{k}, \\ |\boldsymbol{k}|<k_c}} \hat{\tilde{u}}_r(\boldsymbol{p}, t)\hat{\tilde{u}}_m(\boldsymbol{q}, t), \tag{2.16}$$

$$F^s_j(\boldsymbol{k}, t) = -\mathrm{i}k_m \boldsymbol{P}_{jr}(\boldsymbol{k}) \sum_{\substack{\boldsymbol{p}+\boldsymbol{q}=\boldsymbol{k}, \\ |\boldsymbol{k}|<k_c, \max\{|\boldsymbol{p}|, |\boldsymbol{q}|\}>k_c}} \hat{u}_r(\boldsymbol{p}, t)\hat{u}_m(\boldsymbol{q}, t), \tag{2.17}$$

in which $\boldsymbol{F}^s$ is unknown and needs to be modelled using SGS models. In a similar way, (2.15) could be divided into the filtered term $\bar{J}$ and the subgrid term J^s, for which the latter is unknown and should be modelled to close the problem.

2.3. *SGS models*

Most SGS models are based on the eddy viscosity assumption, which is based on the turbulent-viscosity hypothesis (e.g. Pope 2000). In this point of view, the nonlinear subgrid terms are related to the filtered physical variables or the filtered Fourier coefficients through an eddy viscosity term in physical or wavenumber space, respectively. We consider two SGS models here: the Smagorinsky (1963) model, which is local in physical space and damps resolved regions with strong rate of strain; and the Kraichnan (1976) model, which is spectrally local and damps mainly the smallest resolved length scales.

2.3.1. *The Smagorinsky model (physical space)*

The deviatoric part of the subgrid flux $\boldsymbol{\tau}^r$ is related to the filtered rate of strain $\bar{s}_{ij} = 1/2(\partial \bar{u}_i/\partial x_j + \partial \bar{u}_j/\partial x_i)$ using the eddy viscosity coefficient ν_r, as

$$\tau^r_{ij}(\boldsymbol{x}, t) = -2\nu_r(\boldsymbol{x}, t)\bar{s}_{ij}(\boldsymbol{x}, t). \tag{2.18}$$

Similarly, the subgrid density flux $\boldsymbol{h}$ is modelled by

$$h_j(\boldsymbol{x}, t) = -\frac{2}{Pr_t}\nu_r(\boldsymbol{x}, t)\frac{\partial}{\partial x_j}\bar{\rho}(\boldsymbol{x}, t), \tag{2.19}$$

where Pr_t is the turbulent Prandtl number. Smagorinsky (1963) suggested a model for the eddy viscosity coefficient for which ν_r is related to the grid spacing Δ and the characteristic filtered rate of strain $\bar{S} = (2\bar{s}_{ij}\bar{s}_{ij})^{1/2}$, through the relation

$$\nu_r(\boldsymbol{x}, t) = (c_s\Delta)^2\bar{S}(\boldsymbol{x}, t), \tag{2.20}$$

where c_s is the Smagorinsky coefficient. Lilly (1967) has shown that (2.20) is an applicable model for LES of three-dimensional turbulence. An estimate of $c_s \approx 0.17$ was made (Lilly 1967; Meneveau & Katz 2000; Pope 2000) for a Kolmogorov isotropic inertial subrange with a sharp spectral filter.

2.3.2. *The Kraichnan model (wavenumber space)*

Kraichnan (1976) suggested the spectral eddy viscosity idea to model the nonlinear subgrid term $\boldsymbol{F}^s$ as (using the notation of Pope 2000)

$$F_j^s(\boldsymbol{k}, t) = -\nu_e(k|k_c)k^2\hat{\bar{u}}_j(\boldsymbol{k}, t), \tag{2.21}$$

where $\nu_e(k|k_c)$ is the spectral eddy viscosity function. Similarly, the subgrid term J^s is related to the filtered Fourier coefficient $\hat{\bar{\rho}}$ as follows

$$J^s(\boldsymbol{k}, t) = -\frac{1}{Pr_t}\nu_e(k|k_c)k^2\hat{\bar{\rho}}(\boldsymbol{k}, t). \tag{2.22}$$

Lesieur & Rogallo (1989) proposed the following equation for $\nu_e(k|k_c)$

$$\nu_e(k|k_c) = (0.15 + 5\mathrm{e}^{-3.03k_c/k})\sqrt{\frac{E(k_c, t)}{k_c}}, \tag{2.23}$$

where $E(k_c, t)$ is the kinetic energy spectrum at the cutoff wavenumber k_c. It is important to note that for $k \ll k_c$,

$$\nu_e(k|k_c) \sim 0.15\sqrt{\frac{E(k_c, t)}{k_c}}. \tag{2.24}$$

Hence, the eddy viscosity coefficient $\nu_e(k|k_c)$ is independent of $\boldsymbol{k}$ for small wavenumbers. By contrast with the Smagorinsky approach, the Kraichnan model has the advantage that it preferentially damps small length scales; however, it is only practical for idealized simulations with triply periodic spectral codes.

The turbulent Prandtl number Pr_t is usually assumed to be constant (e.g. Lesieur 1990; Batchelor, Canuto & Chasnov 1992; Siegel & Domaradzki 1994). This assumption along with the assumption of constant buoyancy frequency N (e.g. Riley & de Bruyn Kops 2003; Waite & Bartello 2004; Brethouwer *et al.* 2007; Waite 2011; Khani & Waite 2013; Waite 2014) will also be employed in current study.

3. Methodology

LES of forced stratified turbulence is studied in this paper. Idealized simulations of vortically-forced stratified turbulence in a cubic domain with length $L = 2\pi$ is considered. Random forcing of barotropic vortical modes in the wavenumber band $|k_h - k_f| \leqslant 1$ is applied, where k_f is the forcing wavenumber (following e.g.

Herring & Métais 1989; Waite & Bartello 2004; Waite 2011). The forcing is AR(1) red noise, uncorrelated in $\boldsymbol{k}$, and with a correlation time scale of 10 timesteps. The forcing amplitude is a quadratic function of the horizontal wavenumber k_h centred in the forcing band. The forcing amplitude is the same for all simulations, apart from a factor of $\Delta t^{-1/2}$, which leads to an approximately fixed average forcing power in all cases. The spectral transform method with cubic truncation is applied for discretization in space. The two-thirds rule (e.g. Durran 2010) is applied to eliminate aliasing errors, meaning that the cutoff wavenumber k_c is

$$k_c = \pi \frac{2n}{3L}, \tag{3.1}$$

where n is the number of grid points in the x, y and z directions. We get the effective resolution $\Delta = 1.5L/n$ by using (3.1) in (2.4). The third-order Adams–Bashforth scheme is employed for time stepping.

We compare our LES results with those obtained using hyperviscosity and hyperdiffusivity, which are commonly employed to mimic large Reynolds number flows in place of traditional LES schemes. These dissipation operators are of forms

$$D_u = \nu_m (-1)^{m+1} \nabla^{2m}, \tag{3.2}$$

$$D_b = \kappa_m (-1)^{m+1} \nabla^{2m}, \tag{3.3}$$

respectively, where ν_m and κ_m are the hyperviscosity and hyperdiffusivity coefficients (see e.g. Waite & Bartello 2004). We set $\nu_m = \kappa_m$, and use $m = 4$ (as in e.g. Bartello, Métais & Lesieur 1996; Waite & Bartello 2004; Waite 2011). The modified Kolmogorov wavenumber in the hyperviscosity case is as follows

$$k_d = \left(\frac{\epsilon}{\nu_4^3} \right)^{1/22}. \tag{3.4}$$

For a given resolution, the hyperviscosity coefficient is chosen to be as small as possible while still adequately resolving k_d. The implicit trapezoidal method is applied for time stepping of the dissipation term in the hyperviscosity and hyperdiffusivity simulations.

Following previous studies of forced stratified turbulence (e.g. Waite & Bartello 2004; Waite 2011) we spin up our simulations with relatively low resolution ($n = 256$) and hyperviscosity from time 0 to 300 (corresponding to around 30 forcing time scales; see below), and then use these low-resolution results as initial conditions for higher-resolution LES from time 300 to 450. Resolutions from $n = 256$ to $n = 768$ are considered.

The Buoyancy frequency N ranges from 2 to 6, which are chosen to be strongly stratified; indeed, the corresponding Froude numbers ranges from 0.0024 to 0.014, as will be presented in the next section. Similar ranges for Froude numbers have been considered in previous numerical studies of stratified turbulence (e.g. Riley & de Bruyn Kops 2003; Hebert & de Bruyn Kops 2006*a*,*b*; Khani & Waite 2013). These Froude numbers are a little larger than typical values of the atmospheric mesoscale ($\sim 10^{-4}$; e.g. Brune & Becker 2013) but meet the criteria for strongly stratified turbulence (Lindborg 2006). The corresponding Ozmidov scales are not resolved in these experiments; however, previous hyperviscosity simulations have shown and argued that it is sufficient to resolve the buoyancy scale (e.g. Waite & Bartello

2004; Lindborg 2006; Brethouwer *et al.* 2007). The forcing amplitude gives a typical dissipation rate of 10^{-4} which, when combined with the forcing wavenumber k_f, gives a forcing time scale $t_f \sim 10$. We use $\sqrt{\langle E(t)\rangle}$ in place of u_{rms} since the vertical kinetic energy is much smaller than the horizontal. The turbulent Prandtl number $Pr_t = 1$ for LES and the forcing wavenumber $k_f = 3$ are also considered in this study. Tables 1 and 2 show a list of parameters and averaged variables for hyperviscosity simulations and LES, respectively.

4. Results and discussion

4.1. *Overview of simulations*

Figure 1 shows time series of kinetic energy and dissipation rates for the hyperviscosity simulations (*a*,*b*), the Smagorinsky LES (*c*,*d*), and the Kraichnan LES (*e*,*f*), when $0 \leqslant t \leqslant 450$. The simulations appear to have reached statistical stationarity for $375 \leqslant t \leqslant 450$, which is the time period for averaging of the results that follow. The time series of the kinetic energy dissipation rates $\epsilon(t)$ exhibit a discontinuity at $t = 300$, due to the change in resolution and SGS mechanism at this time. Interestingly, the Smagorinsky and Kraichnan dissipation rates are similar, and are both close to the lower-resolution hyperviscosity case (tables 1 and 2, where the angle brackets $\langle\cdot\rangle$ denote time averaging). We will discuss this dependence on SGS scheme in § 4.2. In addition, increasing the stratification increases kinetic energy and u_{rms} (tables 1 and 2).

4.2. *Energy spectra*

In this section, we study effects of the grid spacing in different SGS models on the energy and dissipation spectra. In figure 2, averaged total, horizontal and vertical wavenumber kinetic energy are shown for the highest-resolution simulations. Kinetic energy spectra in terms of total, horizontal and vertical wavenumbers k, k_h and k_v are computed by binning over wavevectors in the usual way (e.g. Waite & Bartello 2004; Waite 2011; Kimura & Herring 2012; Khani & Waite 2013). Hyperviscosity simulations (i.e. figure 2*a*,*b*) have long tails for k, k_h, $k_v \gtrsim 100$, showing the hyperviscous dissipation range. The total wavenumber energy spectra are very similar to the vertical spectra except for the peak around the forcing wavenumber k_f, hence we will focus on $\langle E(k_h)\rangle$ and $\langle E(k_v)\rangle$.

The averaged vertical wavenumber spectra in all cases are peaked at $k_v \approx 20$ for $N = 2$ and $k_v \approx 40$ for $N = 6$, illustrating that the peak location changes with N. This behaviour is consistent with previous results which show that the characteristic vertical wavenumber is the buoyancy wavenumber $k_b = N/u_{rms}$, provided it is not in the dissipation range (e.g. Waite & Bartello 2004; Waite 2011; k_b is denoted by arrows in figure 2). The averaged vertical wavenumber spectrum is approximately flat up to the wavenumber at which the spectrum is peaked (as also seen in e.g. Herring & Métais 1989; Waite & Bartello 2004), beyond which it decays with a slope of around -2.4, -3.4 and -2.8 for the hyperviscosity simulation, the Smagorinsky LES and the Kraichnan LES, respectively, when $N = 2$. Similarly, the vertical wavenumber spectrum decays with a slope of around -1.2, -3.8 and -2 for the hyperviscosity simulation, the Smagorinsky LES and the Kraichnan LES, respectively, when $N = 6$. We use the least-squares method to measure spectral slopes over $40 \leqslant k_v \leqslant 100$.

The averaged horizontal wavenumber energy spectra are peaked around the forcing wavenumber $k_f = 3$. With hyperviscosity, the slope is around -1 for $N = 2$ and -2 for

https://doi.org/10.1017/jfm.2014.381 Published online by Cambridge University Press

Hyperviscosity	N	n	ν_4	k_{max}	k_b	k_d	k_o	$\langle\epsilon\rangle$	$\langle E(t)\rangle$	Fr_h	Δt
h7N2	2	768	8.42×10^{-19}	256	30	186	402	5.0×10^{-5}	0.0045	0.0055	0.0060
h7N4	4	768	8.42×10^{-19}	256	58	187	1042	5.9×10^{-5}	0.0048	0.0031	0.0055
h7N6	6	768	8.42×10^{-19}	256	77	191	1565	8.8×10^{-5}	0.0060	0.0024	0.0050
h2N2	2	256	3.18×10^{-15}	85	29	62	325	7.6×10^{-5}	0.0047	0.0080	0.0180
h2N4	4	256	3.18×10^{-15}	85	51	62	771	1.1×10^{-4}	0.0061	0.0044	0.0165
h2N6	6	256	3.18×10^{-15}	85	72	63	1374	1.1×10^{-4}	0.0070	0.0027	0.0150

TABLE 1. List of numerical simulations with hyperviscosity.

https://doi.org/10.1017/jfm.2014.381 Published online by Cambridge University Press

Smagorinsky	N	n	k_b	k_c	k_o	$\langle\epsilon\rangle$	$\langle E(t)\rangle$	Fr_h	k_c/k_b	Δ/L_b	Δt
S7N2	2	768	32	254	286	9.8×10^{-5}	0.0039	0.012	7.94	0.063	0.0060
S7N4	4	768	62	254	773	1.1×10^{-4}	0.0043	0.006	4.10	0.122	0.0055
S7N6	6	768	86	254	1391	1.1×10^{-4}	0.0048	0.004	2.95	0.169	0.0050
S5N2	2	512	31	168	262	1.2×10^{-4}	0.0042	0.014	5.42	0.092	0.0090
S5N4	4	512	57	168	710	1.3×10^{-4}	0.0050	0.006	2.95	0.169	0.0082
S2N2	2	256	32	83	282	1.0×10^{-4}	0.0040	0.013	2.59	0.193	0.0180
Kraichnan	N	n	k_b	k_c	k_o	$\langle\epsilon\rangle$	$\langle E(t)\rangle$	Fr_h	k_c/k_b	Δ/L_b	Δt
K7N2	2	768	30	254	266	1.1×10^{-4}	0.0045	0.012	8.47	0.059	0.0060
K7N6	6	768	82	254	1368	1.2×10^{-4}	0.0053	0.004	3.10	0.161	0.0050
K2N2	2	256	31	83	272	1.1×10^{-4}	0.0042	0.013	2.68	0.186	0.0180
K2N4	4	256	57	83	738	1.2×10^{-4}	0.0050	0.006	1.45	0.345	0.0165
K2N6	6	256	78	83	1270	1.3×10^{-4}	0.0060	0.004	1.06	0.472	0.0150

TABLE 2. List of numerical simulations with LES.

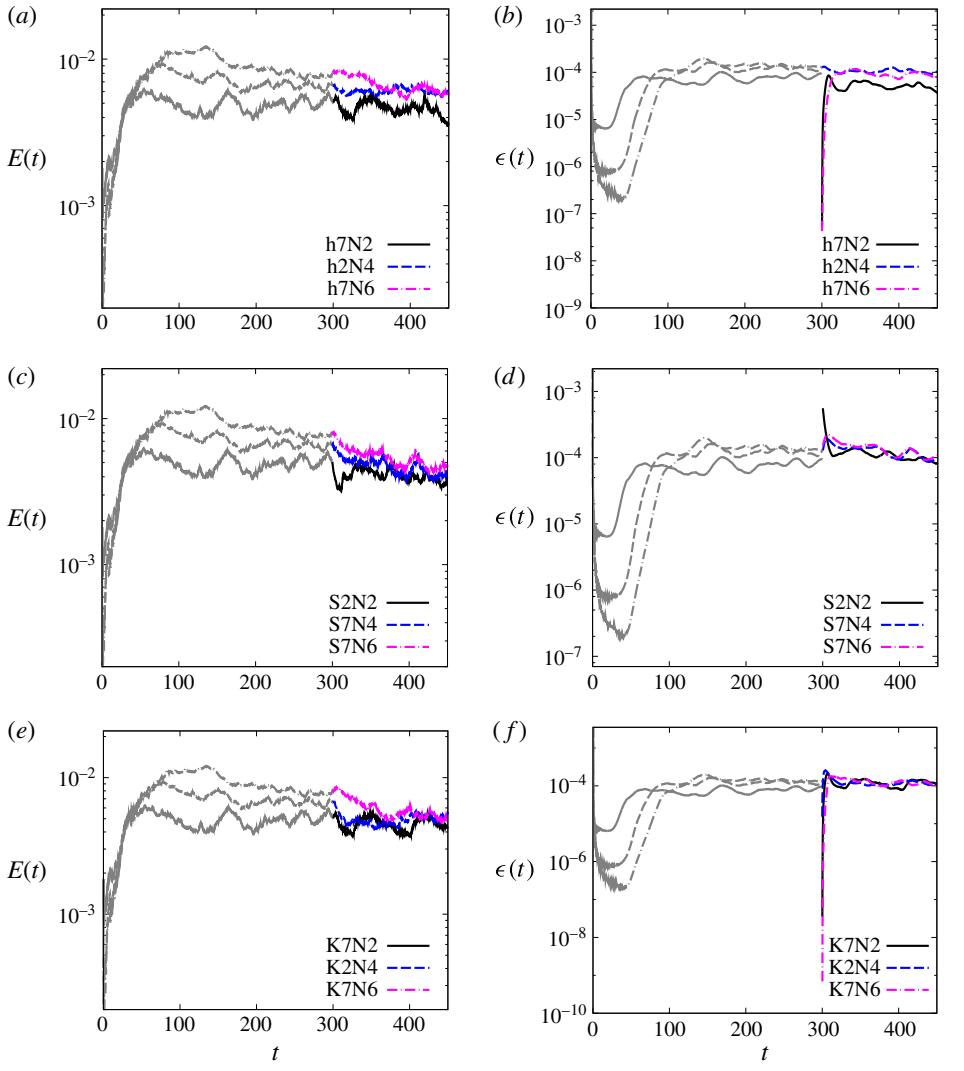

FIGURE 1. (Colour online) Time series of kinetic energy (*a,c,e*) and the kinetic energy dissipation rate (*b,d,f*) for (*a,b*) the hyperviscosity simulations, (*c,d*) the Smagorinsky LES and (*e,f*) the Kraichnan LES. The grey curves over $0 \leqslant t \leqslant 300$ are the low-resolution hyperviscosity simulations with the corresponding buoyancy frequency N.

$N = 6$ (over $10 \leqslant k_h \leqslant 30$ and $10 \leqslant k_h \leqslant 50$, respectively). For the same ranges of k_h, the spectral slopes in the Smagorinsky LES are approximately -1.5 for $N = 2$ and -4 for $N = 6$ (figure 2*c,d*). Similarly, the Kraichnan LES gives slopes of -1.4 and -1.9 for $N = 2$ and $N = 6$, respectively (figure 2*e,f*). As a result, increased stratification steepens the spectra in the hyperviscosity simulations and the LES. In addition, at fixed resolution and N, different SGS models give different slopes; the Smagorinsky simulations are consistently steeper than those using the Kraichnan model. Overall, hyperviscosity and LES give slopes that are shallower than $-5/3$ for $N = 2$. For $N = 6$ however, slopes are steeper than $-5/3$. In addition, the averaged horizontal

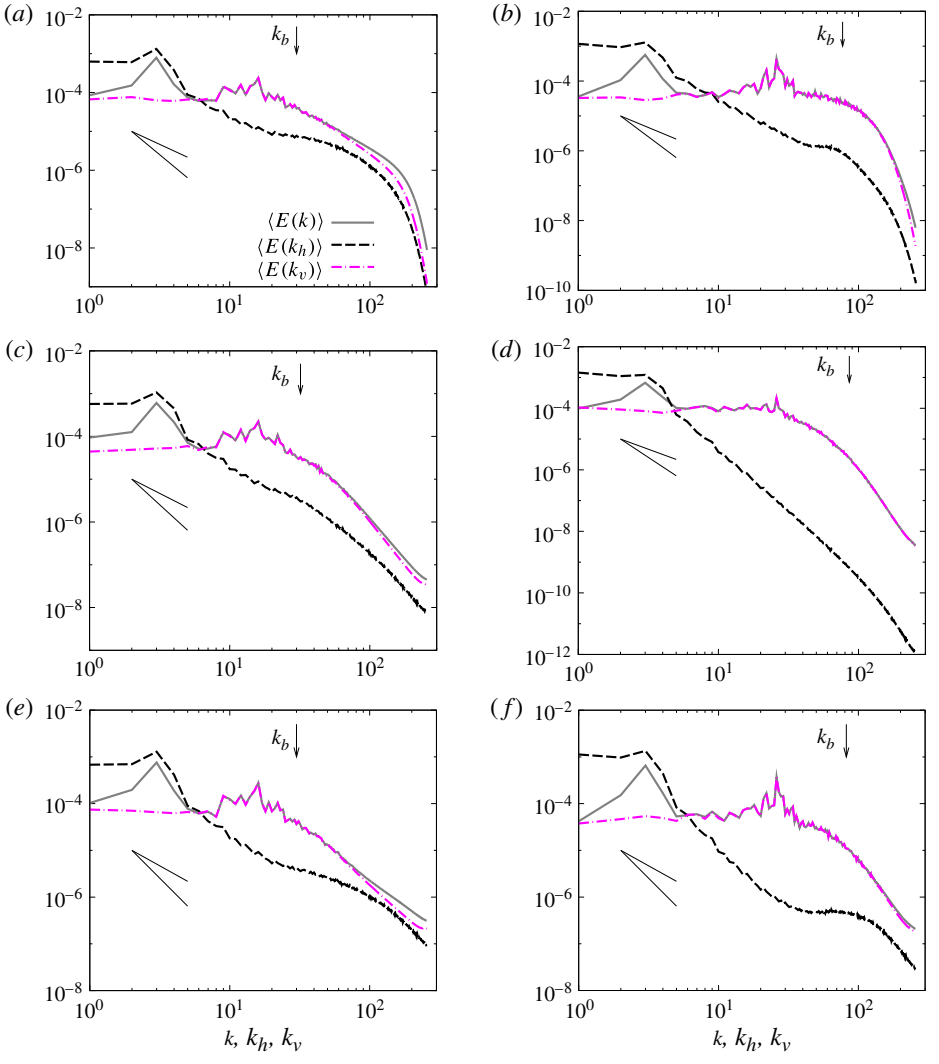

FIGURE 2. (Colour online) The averaged total, horizontal and vertical wavenumber energy spectra with resolution $n = 768$ for (a,b) the hyperviscosity simulations, (c,d) the Smagorinsky LES, and (e,f) the Kraichnan LES, for $N = 2$ (a,c,e) and $N = 6$ (b,d,f). Spectra are averaged over $375 \leqslant t \leqslant 450$. Arrows correspond to the buoyancy wavenumber k_b and the forcing wavenumber is $k = 3$. The black solid line segments show $-5/3$ and -3 slopes.

wavenumber energy spectra exhibit a bump at around the buoyancy wavenumber k_b (see arrows in figure 2) except for the Smagorinsky LES with $N = 6$ (figure 2*d*).

Figure 3 shows the horizontal and vertical wavenumber spectra of SGS energy transfer (i.e. eddy dissipation spectra) for the low- and high-resolution Kraichnan and Smagorinsky LES at $t = 450$. Interestingly, for both SGS models, the maximum dissipation happens at large horizontal and small vertical scales, which show an anisotropic energy transfer from resolved scales towards SGS motions (similar trends are seen in the stratified SGS energy transfer spectra in DNS of Khani & Waite 2013).

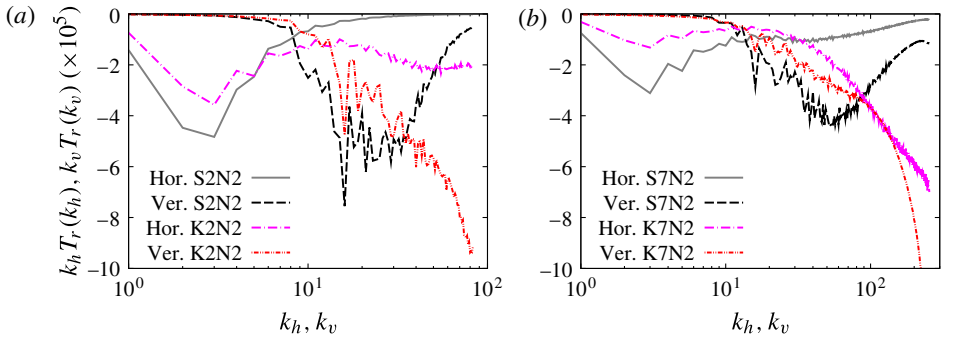

FIGURE 3. (Colour online) The horizontal and vertical wavenumber spectra of SGS energy transfer for the Smagorinsky and Kraichnan LES at $t = 450$. Low- and high-resolution cases are shown in (*a*) and (*b*), respectively. The spectra are multiplied by wavenumber in order to preserve area on the log-linear axes.

As a result, although the Smagorinsky and Kraichnan eddy viscosities are defined isotropically, the SGS energy transfer spectra inherit the anisotropy of the resolved motions. For both high- and low-resolution cases, the Smagorinsky LES shows a larger peak in the horizontal wavenumber SGS energy transfer spectra, implying that the Smagorinsky model is much more dissipative than the Kraichnan model (figure 3). The same conclusions hold for the vertical wavenumber SGS energy transfer spectra as well. Meanwhile, the Kraichnan LES shows a cusp around k_c in the vertical SGS energy spectra and the high-resolution horizontal SGS spectra, implying that the Kraichnan model is more consistent with the DNS of Khani & Waite (2013). In addition, the horizontal and vertical SGS energy transfer spectra for the low-resolution Kraichnan case with $N = 2$ are remarkably similar to those of the corresponding high-resolution Smagorinsky LES far from the cutoff wavenumber k_c. As a result, the non-local horizontal and vertical SGS energy transfers in the high-resolution Smagorinsky LES are very similar to those of the low-resolution Kraichnan model.

To make a quantitative comparison of the SGS terms from the two LES approaches, the effective spectral eddy viscosity of the Smagorinsky LES at $t = 450$ is shown in figure 4. We compute $\nu_r(k)$ by diving the absolute value of the spherical SGS energy transfer $T_r(k)$ of the Smagorinsky LES by $2k^2E(k)$. There is a broad range of k/k_c with a plateau of almost constant $\nu_r(k)$, and no cusp is seen around $k = k_c$. The effective spectral eddy viscosity from the Smagorinsky model is quite different from actual effective eddy viscosity measured in high-resolution DNS of stratified turbulence, in which a cusp around the cutoff wavenumber k_c is a dominant feature (Khani & Waite 2013). For comparison, the Kraichnan eddy viscosity $\nu_e(k)$ for the case with $n = 256$ and $N = 2$ is also shown in figure 4; it exhibits a lower plateau and a large cusp, in better agreement with DNS of Khani & Waite (2013). The plateau in the low-resolution Smagorinsky case is almost three times larger than the Kraichnan plateau. Interestingly, the low-resolution Kraichnan plateau is very close to the plateaus of the high-resolution Smagorinsky simulations. These results are consistent with the energy and eddy dissipation spectra, which show that the Smagorinsky model is much more dissipative than the Kraichnan model.

Figure 5 shows compensated horizontal energy spectra (in which the horizontal spectra are normalized by $k_h^{-5/3}\langle\epsilon\rangle^{2/3}$) for the hyperviscosity simulations and LES

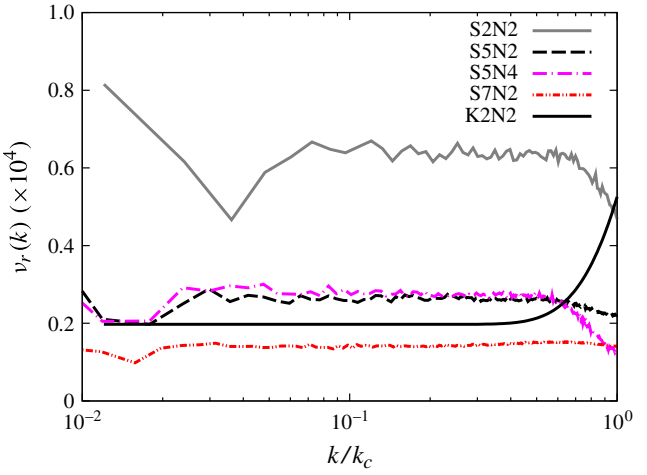

FIGURE 4. (Colour online) Effective spectral eddy viscosity for the Smagorinsky cases along with the Kraichnan eddy viscosity ν_e for the low-resolution case with $N = 2$. For computing eddy viscosities, results at $t = 450$ are used; the horizontal axis is normalized by the cutoff wavenumber k_c.

when $N = 2$, 4 and 6. As in figure 2, arrows show the location of the buoyancy wavenumber k_b. In figure 5(*a*), the compensated horizontal wavenumber energy spectrum for the high-resolution hyperviscosity case is almost constant for $6 \lesssim k_h \lesssim 30$, which is consistent with an inertial subrange with a slope close to $-5/3$. A bump is visible at $k_h \approx 30$, which is around the buoyancy wavenumber k_b. Similar bumps have been investigated in recent hyperviscosity simulations and DNS (Laval, McWilliams & Dubrulle 2003; Waite 2011; Augier *et al.* 2012; Waite 2014). A similar constant inertial subrange and bump at $k_h \sim k_b$ are also seen in the other simulations in figure 5(*a*) except for the low-resolution Smagorinsky LES. Interestingly, the Smagorinsky spectrum with $n = 768$ looks very similar to the Kraichnan spectrum with $n = 256$; the inertial range slope and amplitude, and the bump near k_b, are nearly identical. In other words, the low-resolution Kraichnan simulation reproduces the higher-resolution Smagorinsky simulation, despite having a grid spacing three times as coarse.

The results with higher stratification are similar. For $N = 4$ (figure 5*b*) an almost flat inertial subrange over $6 \lesssim k_h \lesssim 50$ is seen for the high-resolution hyperviscosity case, which is followed by a bump at around $k_h = 60$ (very close to k_b). Other simulations in this panel, except the low-resolution hyperviscosity case (i.e. h2N4) and the middle-resolution Smagorinsky case (i.e. S5N4), show a very short inertial subrange along with a little bump at around k_b. Once again, the high-resolution Smagorinsky spectrum looks like the low-resolution Kraichnan up to $k_h \approx 30$. In figure 5(*c*), the high-resolution hyperviscosity and Kraichnan cases with $N = 6$ show the constant inertial subrange at $6 \lesssim k_h \lesssim 60$ and a bump at $k_h \sim k_b$. However, other simulations in this panel show a very steep compensated spectrum. Like in figure 5(*a*, *b*), figure 5(*c*) demonstrates that the low-resolution Kraichnan LES looks like the high-resolution Smagorinsky LES. In addition, the hyperviscous simulation is more dissipative than the Kraichnan LES at very large wavenumbers (figure 5). At large wavenumbers, i.e. $k \gtrsim 100$, the effective eddy viscosity given by the hyperviscosity $\nu_m k^{2m-2}$ is larger

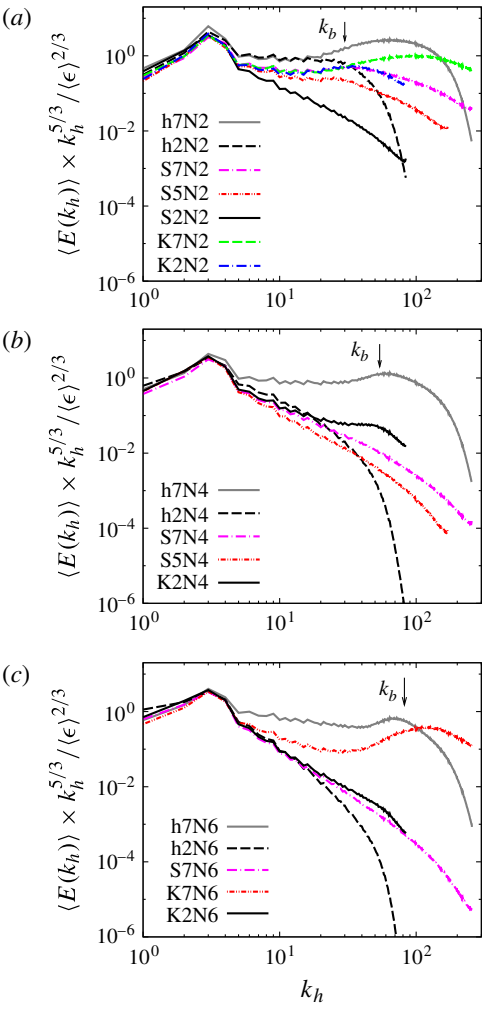

FIGURE 5. (Colour online) The averaged compensated horizontal energy spectra: (*a*) $N = 2$, (*b*) $N = 4$ and (*c*) $N = 6$. Spectra are averaged over $375 \leqslant t \leqslant 450$. Arrows correspond to the buoyancy wavenumber k_b and the forcing wavenumber is at $k = 3$.

than ν_e, hence the hyperviscosity simulation is more strongly damped at large k. As a result, the Kraichnan LES seems to give more reasonable results compared with hyperviscosity at very large wavenumbers. In addition, the potential energy spectra (not shown here) also show peaks and bumps around k_b in the vertical and horizontal wavenumber spectra, respectively.

4.3. *KH instabilities and the Richardson number*

Figure 6 shows the y-component of vorticity $\bar{\omega}_y = (\partial\bar{u}/\partial z - \partial\bar{w}/\partial x)$ on the $x - z$ plane at $y = 0.25$ and $t = 450$ for the high-resolution Kraichnan LES. Vortices are lengthened in the horizontal direction and layered in the vertical. For the lower stratification (figure 6*a*), intermittent instabilities and KH billows are visible between the layers. Stronger stratification (figure 6*b*) shows a more strongly layered structure with fewer

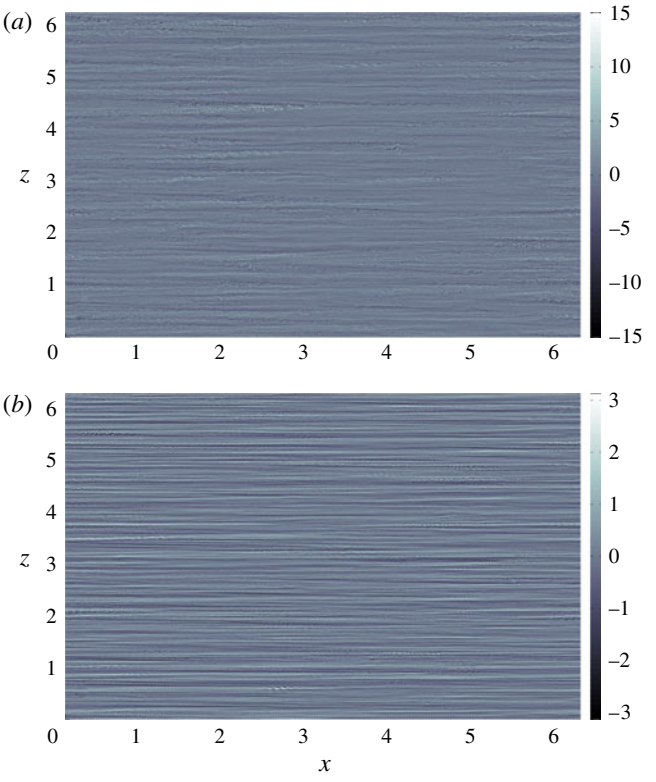

FIGURE 6. (Colour online) Vorticity field in y direction $\bar{\omega}_y$ on the x–z plane at $y = 0.25$ and $t = 450$ for the high-resolution Kraichnan LES: (*a*) $N = 2$ and (*b*) $N = 6$. Vorticity fields are normalized by the corresponding buoyancy frequency N.

regions of KH instability. Figure 7 shows $\bar{\omega}_y$ for the high-resolution Smagorinsky LES. As in the Kraichnan LES, the lower stratification (figure 7*a*) shows a layered vertical structures with KH instabilities. No instabilities are visible in the more strongly stratified case (figure 7*b*). According to figures 6 and 7, increased stratification at fixed resolution and SGS scheme inhibits KH instabilities, since the thinner layers in the more strongly stratified case are more influenced by dissipation (Hebert & de Bruyn Kops 2006*a*; Brethouwer *et al.* 2007). In addition, KH instabilities are inhibited in the Smagorinsky simulation relative to the Kraichnan and hyperviscosity cases at the same stratification and resolution, suggesting that the Smagorinsky case is the most dissipative.

The above results suggest that there is a bump around k_b in the horizontal wavenumber energy spectrum only when KH instabilities are visible in the vorticity plots. This hypothesis has been proposed in several studies (Laval *et al.* 2003; Waite 2011; Augier *et al.* 2012; Waite 2014). To further investigate this relationship in LES and to investigate the influence of different SGS models, we consider the Richardson number in our simulation. The Richardson number shows the competition between stratification, which stabilizes flow, and the vertical shear of horizontal motions, which excites instabilities. The local Richardson number is given as follows

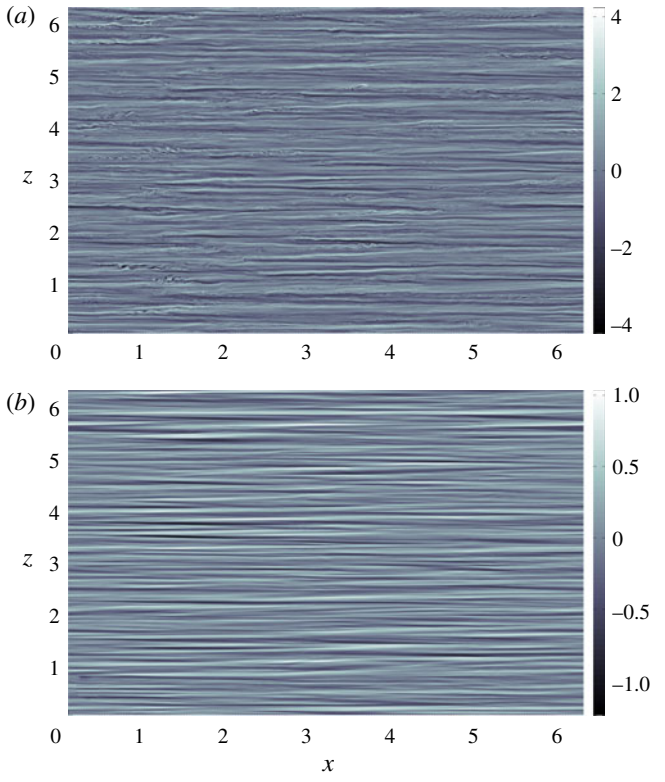

FIGURE 7. (Colour online) Vorticity field in y direction $\bar{\omega}_y$ on the x–z plane at $y = 0.25$ and $t = 450$ for the high-resolution Smagorinsky LES: (*a*) $N = 2$ and (*b*) $N = 6$. Vorticity fields are normalized by the corresponding buoyancy frequency N.

$$Ri = \frac{N^2 - \dfrac{g}{\rho_0}\dfrac{\partial \bar{\rho}}{\partial z}}{\left(\dfrac{\partial \bar{u}}{\partial z}\right)^2 + \left(\dfrac{\partial \bar{v}}{\partial z}\right)^2}, \tag{4.1}$$

in which the numerator is the buoyancy frequency squared from the total (background plus perturbation) density; and g and ρ_0 are gravity and the reference density, respectively. The classical necessary condition for instability $Ri < 1/4$ is strictly applicable only for parallel shear flow, but is nevertheless commonly employed to diagnose regions of KH instabilities in more complicated flows (e.g. Riley & de Bruyn Kops 2003; Augier & Billant 2011, which considered decaying stratified turbulence and breakdown of vortex, respectively). As a result, we consider the structure and distribution of Ri, with the understanding that more points with $Ri < 1/4$ might suggest more regions with KH instabilities. Furthermore, $Ri < 0$ implies overturning. The vorticity plot shows a large-scale layered structure with intermittent smaller-scale structures (e.g. figure 7*a*). Small-scale vorticity structures correspond to regions with small Ri, < 0.25 and in many cases < 0 (see the Ri field in figure 8), consistent with KH instabilities in different stages of evolution, as has been discussed elsewhere (e.g. Riley & de Bruyn Kops 2003). Figure 8 shows the local Richardson number in x–z plane for the high-resolution Smagorinsky simulation with $N = 2$ (where the

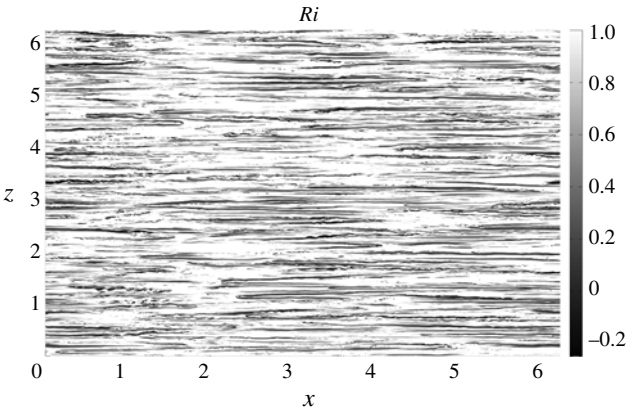

FIGURE 8. The local Richardson number Ri field on the x–z plane at $y = 0.25$ and $t = 450$ for the Smagorinsky case with $N = 2$ and $n = 768$. The Richardson number values are restricted between -0.25 and 1.

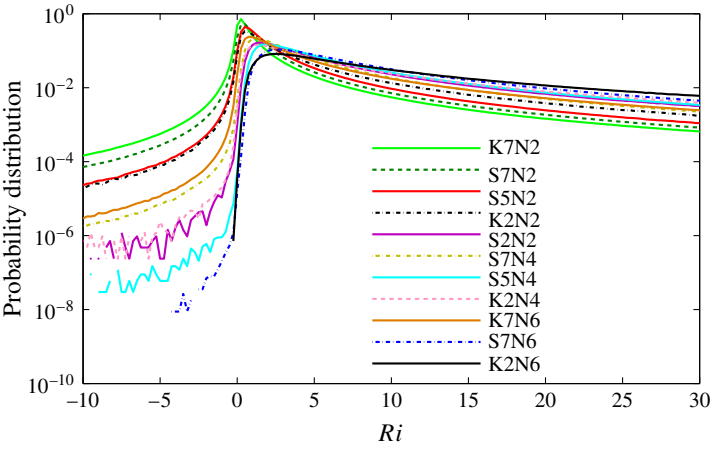

FIGURE 9. (Colour online) Histograms of the local Richardson number Ri at $t = 450$. Only the segment $-10 \leqslant Ri \leqslant 30$ is shown. Histograms are normalized by bin size to give probability distributions, and are computed with 1000 bins over $-50 < Ri < 200$ ($\Delta Ri = 0.25$).

vorticity plot for that is shown in figure 7*a*). We have shown only Ri values between $-1/4$ to 1. Intermittent spots with darker colours correspond to regions with $Ri < 1/4$, which show high shear between the layers. This figure shows that the small-scale disturbances in the vorticity field, many of which resemble KH instabilities, are colocated with regions of small $Ri < 1/4$, including many points with $Ri < 0$.

For an overview of the Richardson number in all simulations, figure 9 shows histograms of Ri for the LES at $t = 450$. For clarity, only the range $-10 \leqslant Ri \leqslant 30$ is shown. Figure 9 presents results for different resolutions, SGS models and buoyancy frequencies. Decreasing the resolution from $n = 768$ to 256 causes the histograms drop off rapidly for negative Ri and causes the peak around $Ri = 0$ to decrease. In addition, the Richardson number histogram show a long positive tail. Figure 9 shows that at fixed resolution, increased stratification reduces the numbers of points with negative

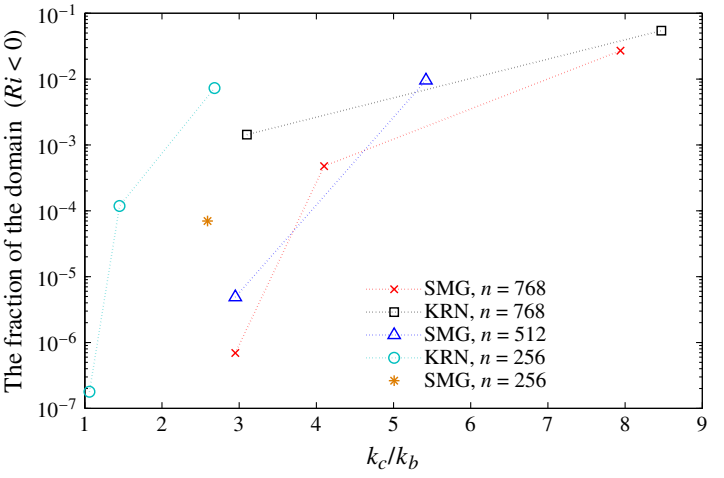

FIGURE 10. (Colour online) The fraction of the domain with $Ri < 0$ as a function of the ratio k_c/k_b for the Smagorinsky and Kraichnan LES at different resolutions.

Ri and decreases the peak around $Ri = 0$, e.g. see the high-resolution Kraichnan case with $N = 2$ (the solid green line) versus that with $N = 6$ (the solid brown line), or the high-resolution Smagorinsky case with $N = 2$ (the dashed green line) versus that with $N = 6$ (the dash dotted blue line). Furthermore, in the low-resolution Kraichnan case with $N = 6$ (i.e. K2N6), overturning is completely suppressed because there are no points with negative *Ri*. As a result, by decreasing the resolution or increasing the stratification, the number of points with negative *Ri* decreases, and regions of small-scale instability and overturning are eliminated (e.g. figure 7*b*). In addition, at fixed resolution and buoyancy frequency, different SGS models result in different Richardson number histograms. For example, the high-resolution Kraichnan case with $N = 2$ has a larger numbers of negative *Ri* and a smaller numbers of positive *Ri* compared with the high-resolution Smagorinsky case with $N = 2$, implying that the latter case is more stabilizing than the former one. Similar behaviours are seen in low-resolution cases with $N = 2$ or high-resolution cases with $N = 6$. It is interesting to mention that the *Ri* histograms of the low-resolution Kraichnan case with $N = 2$ and $n = 256$ are very similar to the higher-resolution Smagorinsky cases with $N = 2$ and $n = 512$. Similarly, the *Ri* histogram of Kraichnan cases with $N = 6$ and $n = 256$ are very close to that of Smagorinsky with $N = 6$ and $n = 768$. Overall, the Smagorinsky LES seems much more dissipative than the Kraichnan model, since small-scale instabilities and overturning is suppressed significantly.

Figure 10 shows the fraction of the domain with $Ri < 0$ as a function of k_c/k_b for the Smagorinsky and Kraichnan cases. Increased k_c/k_b at fixed resolution leads to more grid points with negative Richardson numbers (similar trends are also seen for the number of grid points with $0 < Ri < 0.25$; not shown). As a result, increased resolution at fixed stratification or decreased stratification at fixed resolution generates more overturning regions and small-scale instabilities. Even at fixed k_c/k_b, the overturning fractions depends on resolution, with higher resolution yielding smaller fractions. In addition, figure 10 also demonstrates that the fraction of the domain with $Ri < 0$ is higher for the Kraichnan LES comparing with the Smagorinsky case at the same resolution.

4.4. *Discussion*

In this section, we discuss the LES results inferred from §§ 4.1–4.3. First, we summarize the important points from the previous sections.

(i) The horizontal vorticity field shows regions of small-scale instabilities and turbulence for the high-resolution Kraichnan and Smagorinsky cases with $N = 2$ (figures 6*a* and 7*a*). Increased stratification stabilizes the flows, such that no instabilities are seen in for example the high-resolution Smagorinsky simulation with $N = 6$ (figure 7*b*). In addition, these regions of instabilities correspond to regions with small or negative Ri (figure 8).

(ii) The compensated horizontal energy spectra show an approximately $-5/3$ inertial subrange along with a bump at $k_h \sim k_b$ in the high-resolution Kraichnan and Smagorinsky simulations with $N = 2$ and the high-resolution Kraichnan case with $N = 2$, but not for the high-resolution Smagorinsky case with $N = 6$ (figure 5). Increasing the grid spacing shortens the inertial subrange and seems to suppress the bump at k_b.

(iii) Larger numbers of negative Ri are seen in histograms of the local Richardson number in the high-resolution Kraichnan and Smagorinsky simulations with $N = 2$ (figures 9 and 10). Increased stratification causes a rapid drop in points with negative Ri, e.g. the high-resolution Smagorinsky case with $N = 6$. Increasing the grid spacing also leads to a significant decrease in the histogram of negative Ri.

Our numerical experiments show that if the grid spacing is fine enough to capture the bump in the horizontal wavenumber spectrum, then KH instabilities and small and negative Ri are more likely to happen in physical space. This critical resolution seems to depend on L_b and is different for the different SGS models. Table 2 shows the ratio of k_c/k_b and Δ/L_b for the Smagorinsky and Kraichnan SGS simulations. According to the energy spectra in figures 2 and 5 and the Ri histograms in figure 9, the Smagorinsky LES captures small-scale KH instabilities, indicated by a spectral bump near $k_h \sim k_b$ and points with small and negative Ri, for all cases except for the low-resolution case with $N = 2$, the middle resolution case with $N = 4$, and the high-resolution case with $N = 6$. By contrast, the Kraichnan simulations capture this behaviour for all cases except the low-resolution case with $N = 6$. For the low-resolution Kraichnan case with $N = 4$, there is a visible bump in figure 5(*b*), but very few points with small and negative Ri are seen in figure 9. This discrepancy could be due to sampling, since the spectra in figure 5(*b*) are averaged over $375 \leqslant t \leqslant 450$, while this histogram of Ri is instantaneous at $t = 450$. As a result, the minimum resolution for the Smagorinsky simulations is inside the range $0.12L_b \leqslant \Delta < 0.17L_b$ and for the Kraichnan simulations is inside the range $0.34L_b \leqslant \Delta < 0.47L_b$. Hence, the Smagorinsky LES needs to have k_c/k_b almost three times larger than Kraichnan to resolve KH instabilities. We emphasize that both SGS models have to resolve L_b to capture the dynamics of stratified turbulence, but the Smagorinsky model must resolve L_b almost three times better than Kraichnan. Of course, the Kraichnan model only works with spectral methods, but for such simulations, it is a much better choice than the Smagorinsky model.

5. Conclusion

LES of forced stratified turbulence with different resolutions, buoyancy frequencies and SGS models are studied in this paper. The averaged dissipation rates are almost identical for the Smagorinsky and Kraichnan LES, confirming that $\langle \epsilon \rangle$ depends on

the large scales. The averaged vertical energy spectra are flat up to a certain vertical wavenumber, which depends on the buoyancy frequency N. The averaged horizontal energy spectra depends on the grid spacing and if Δ is small enough, the spectra have an almost $-5/3$ slope along with a bump at $k_h \sim k_b$. These spectra are in line with previous work on stratified turbulence using regular or hyper-viscosity (e.g. Waite & Bartello 2004; Lindborg 2006; Brethouwer *et al.* 2007; Waite 2011; Augier *et al.* 2012; Waite 2014). Increased resolution or decreased stratification promotes KH instabilities between vertical layers. Stronger stratification or smaller k_c inhibits these instabilities by shrinking the layer thickness towards the dissipation scale or by increasing the dissipation scale, respectively. These findings are reminiscent of the Re_b criterion for DNS: stronger stratification requires higher resolution, and hence larger effective Reynolds number, to fully capture the dynamics of stratified turbulence.

We present a threshold on the grid spacing Δ for which dynamics of stratified turbulence are captured in LES. Our results show that the Smagorinsky LES needs much smaller (three times) Δ/L_b compared with the Kraichnan simulations, in order to reproduce the bump in the horizontal wavenumber spectrum and the associated regions of small and negative Ri. In addition, at large wavenumbers, the hyperviscosity simulation is more dissipative than the Kraichnan LES with the same resolution. Therefore, for k_b close to k_{max} and k_c, the Kraichnan LES seems to get reasonable results compared to hyperviscosity, where the former captures the bump in the horizontal energy spectrum but the latter does not (e.g. low-resolution hyperviscosity with $N = 4$ versus low-resolution Kraichnan with $N = 4$ in figure 5*b*). These SGS models are isotropic and they clearly fail when $\Delta > L_b$ where the turbulence is strongly anisotropic. Interestingly, classical theory predicts isotropy below the Ozmidov scale L_o rather than the buoyancy scale L_b, but nevertheless, these isotropic SGS models work well for Δ sufficiently less than L_b but still greater than L_o.

For future work, the performance of LES models beyond the Smagorinsky and Kraichnan schemes should be investigated for stratified turbulence. In particular, the dynamic Smagorinsky model (Germano *et al.* 1991), in which c_s is not constant, has the potential to improve the disappointing performance of the Smagorinsky model seen in this study. Since the dynamics model determines c_s locally and with respect to the dynamics of the structures of flows, it might show better performance than the Smagorinsky model at low resolution, and hence decrease the computational costs. Meanwhile, considering anisotropic eddy viscosity terms, in which the horizontal and vertical deformations are considered separately, is another potential avenue for further work. In addition, we need to ultimately perform very high-resolution DNS of stratified turbulence that resolves a large inertial subrange to obtain a more fundamental understanding of the energy transfer between large and small scales.

Acknowledgements

Computations were performed on the gpc supercomputer at the SciNet HPC Consortium. SciNet is funded by: the Canada Foundation for Innovation under the auspices of Compute Canada; the Government of Ontario; Ontario Research Fund–Research Excellence; and the University of Toronto. Also, this work was made possible by the facilities of the Shared Hierarchical Academic Research Computing Network (SHARCNET: www.sharcnet.ca) and Compute/Calcul Canada. In addition, computing resources from the Mathematics Faculty Computing Facility

of the University of Waterloo are gratefully appreciated. Financial support from the Natural Sciences and Engineering Research Council of Canada is gratefully acknowledged.

REFERENCES

AUGIER, P. & BILLANT, P. 2011 Onest of secondary instabilities on the zigzag instability in stratified fluids. *J. Fluid Mech.* **682**, 120–131.

AUGIER, P., CHOMAZ, J.-M. & BILLANT, P. 2012 Spectral analysis of the transition to turbulence from a dipole in stratified fluid. *J. Fluid Mech.* **713**, 86–108.

BARTELLO, P., MÉTAIS, O. & LESIEUR, M. 1996 Geostrophic versus wave eddy viscosities in atmospheric models. *J. Atmos. Sci.* **53**, 564–571.

BATCHELOR, G. K., CANUTO, V. M. & CHASNOV, J. R. 1992 Homogeneous buoyancy-generated turbulence. *J. Fluid Mech.* **235**, 349–378.

BILLANT, P. & CHOMAZ, J.-M. 2001 Self-similarity of strongly stratified inviscid flows. *Phys. Fluids* **13** (6), 1645–1651.

BRETHOUWER, G., BILLANT, P., LINDBORG, E. & CHOMAZ, J.-M. 2007 Scaling analysis and simulation of strongly stratified turbulent flows. *J. Fluid Mech.* **585**, 343–368.

BRUNE, S. & BECKER, E. 2013 Indications of stratified turbulence in a mechanistic GCM. *J. Atmos. Sci.* **70**, 231–247.

CARNEVALE, G. F., BRISCOLINI, M. & ORLANDI, P. 2001 Buoyancy- to inertial-range transition in forced stratified turbulence. *J. Fluid Mech.* **427**, 205–239.

DURRAN, D. R. 2010 *Numerical Methods for Fluid Dynamics with Application to Geophysics*. Springer.

GARGETT, A. E., OSBORN, T. R. & NASMYTH, P. W. 1984 Local isotropy and the decay of turbulence in a stratified fluid. *J. Fluid Mech.* **144**, 231–280.

GERMANO, M., PIOMELLI, U., MOIN, P. & CABOT, W. H. 1991 A dynamic subgrid-scale eddy viscosity model. *Phys. Fluids* A **3** (7), 1760–1765.

HEBERT, D. A. & DE BRUYN KOPS, S. M. 2006*a* Relationship between vertical shear rate and kinetic energy dissipation rate in stably stratified flows. *Geophys. Res. Lett.* **33**, L06602.

HEBERT, D. A. & DE BRUYN KOPS, S. M. 2006*b* Predicting turbulence in flows with strong stable stratification. *Phys. Fluids* **18**, 066602.

HERRING, J. R. & MÉTAIS, O. 1989 Numerical experiments in forced stably stratified turbulence. *J. Fluid Mech.* **202**, 97–115.

KANG, H. S., CHESTER, S. & MENEVEAU, C. 2003 Decaying turbulence in an active-grid-generated flow and comparisons with large-eddy simulation. *J. Fluid Mech.* **480**, 129–160.

KHANI, S. & WAITE, M. L. 2013 Effective eddy viscosity in stratified turbulence. *J. Turbul.* **14** (7), 49–70.

KIMURA, Y. & HERRING, J. R. 2012 Energy spectra of stably stratified turbulence. *J. Fluid Mech.* **698**, 19–50.

KRAICHNAN, R. H. 1976 Eddy viscosity in two and three dimensions. *J. Atmos. Sci.* **33**, 1521–1536.

LAVAL, J.-P., MCWILLIAMS, J. C. & DUBRULLE, B. 2003 Forced stratified turbulence: successive transition with Reynolds number. *Phys. Rev.* E **68**, 036308.

LEONARD, A. 1974 Energy cascade in large eddy simulation of turbulent fluid flow. *Adv. Geophys.* A **18**, 237–248.

LESIEUR, M. 1990 *Turbulence in Fluids*. Kluwer.

LESIEUR, M. & ROGALLO, R. 1989 Large-eddy simulation of passive scalar diffusion in isotropic turbulence. *Phys. Fluids* A **1** (4), 718–722.

LILLY, D. K. 1967 The representation of small-scale turbulence in numerical simulation experiments. In *NCAR Manuscript*, vol. 281, pp. 99–164. National Center for Atmospheirc Research.

LINDBORG, E. 2006 The energy cascade in strongly stratified fluid. *J. Fluid Mech.* **550**, 207–242.

LUMLEY, J. L. 1964 The spectrum of nearly inertial turbulence in stably stratified fluid. *J. Atmos. Sci.* **21**, 99–102.

MENEVEAU, C. & KATZ, J. 2000 Scale-invariance and turbulence models for large-eddy simulation. *Annu. Rev. Fluid Mech.* **32**, 1–32.

MOIN, P., SQUIRES, K., CABOT, W. H. & LEE, S. 1991 A dynamic subgrid-scale model for compressible turbulence and scalar transport. *Phys. Fluids* A **3** (11), 2746–2757.

PAOLI, R., THOURON, O., ESCOBAR, J., PICOT, J. & CARIOLLE, D. 2013 High-resolution large-eddy simulations of sub-kilometer-scale turbulence in the upper troposphere lower stratoposphere. *Atmos. Chem. Phys. Discuss.* **13**, 31891–31932.

PIOMELLI, U., CABOT, W. H., MOIN, P. & LEE, S. 1991 Subgrid-scale backscatter in turbulent and transitional flows. *Phys. Fluids* A **3** (7), 1766–1771.

POPE, S. B. 2000 *Turbulent Flows*. Cambridge University Press.

REMMLER, S. & HICKEL, S. 2012 Direct and large eddy simulation of stratified turbulence. *Intl J. Heat Fluid Flow* **35**, 13–24.

RILEY, J. J. & DE BRUYN KOPS, S. M. 2003 Dynamics of turbulence strongly influenced by buoyancy. *Phys. Fluids* **15**, 2047–2059.

SIEGEL, D. A. & DOMARADZKI, J. A. 1994 Large-eddy simulation of decaying stably stratified turbulence. *J. Phys. Oceanogr.* **24**, 2353–2386.

SMAGORINSKY, J. 1963 General circulation experiments with the primitive equations. I. The basic experiment. *Mon. Weath. Rev.* **91** (3), 99–164.

SMITH, L. M. & WALEFFE, F. 2002 Generation of slow large scales in forced rotating stratified turbulence. *J. Fluid Mech.* **451**, 145–168.

WAITE, M. L. 2014 Direct numerical simulations of laboratory-scale stratified turbulence. In *Modelling Atmospheric and Oceanic Flows: Insights from Laboratory Experiments* (ed. T. von Larcher & P. Williams), American Geophysical Union.

WAITE, M. L. 2011 Stratified turbulence at the buoyancy scale. *Phys. Fluids* A **23**, 066602.

WAITE, M. L. & BARTELLO, P. 2004 Stratified turbulence dominated by vortical motion. *J. Fluid Mech.* **517**, 281–303.